An analytical model for shear behaviour of bolted rock joints

Shuqi Ma; Zhiye Zhao; Junlong Shang

https://doi.org/10.1016/j.ijrmms.2019.04.005

Abstract:

Rock bolts have been widely used to reinforce the jointed rock mass. Modelling the mechanical shear behaviors of the bolted rock joints are difficult due to the complex interactions between bolts and rock joints. The applied pretension forces combined with the axial loads developed in the bolt act as the normal forces which are applied to the rock joints. However, these combined normal forces are not considered in the existing analytical models. An analytical model is proposed in this study to predict the shear behavior of the bolted rock joints, by taking into account the pretension forces, the axial forces developed in the bolt, the interfacial bond stress between the bolt and grout, and dowel shear loads acting transversely to the bolt axis. The proposed analytical model is able to provide complete curves of the dowel shear loads, axial loads, and the global shear loads as a function of the joint shear displacement. The analytically predicted axial load vs shear displacement curves and the global shear load vs shear displacement curves are verified by available experimental tests. The verification shows that the proposed model has the capacity to predict the global shear load evolution as well as the axial load evolution. The factors such as the pretension forces, the bolt inclination angles, the concrete strength and the rock joint friction are successfully accounted for in the analytical model.

Keywords: *shear behaviour; pretension forces; dowel shear force; bolted rock joints; rock bolt*

1. Introduction

Rock bolts have been widely used to reinforce the fractured rock mass in underground rock excavations and to reduce the deformation of rock slopes. The bolt installation could improve the shear strength of rock joints. The mechanical shear responses of bolted rock joints are complex and associated with three main aspects: the bolt dowel shear forces which act transversely to the bolt axis; the axial forces generated in the bolt when the bolt is dragged towards the joint interface during the shear displacement; and the joint friction properties.

The factors which influence the shear strength of bolted rock joints include joint roughness, rock strength, the interfacial bonding characteristics (such as bolt surface profile and grout properties), bolt properties, bolt installation angles and bolt pretension. Many researchers have investigated these influencing factors using the experimental tests [1-11](Bjurstrom 1974; Dight 1983; Dulacka 1972; Spang and Egger, 1990; Ferrero 1995; Pellet and Egger 1996; Aziz et al. 2003; Grasselli 2005; Jalalifar et al. 2006; Jalalifar and Aziz 2010a and 2010b). During shearing movement, joint surface roughness causes joint dilation, i.e. joint opening, which would lead to higher shear stiffness of the bolted rock joint as higher axial forces are mobilized due to the joint dilation [12](Haas, 1981). The bolted rock joint with a larger compressive strength has a larger shear resistance than soft rock [7, 8, 11](Spang and Egger, 1990; Jalalifar and Aziz 2010a and 2010b). The increase of the bolt diameter could also increase the shear stiffness of the bolted rock joint, so that larger shear loads could be generated with the same shear displacement [11](Spang and Egger, 1990). The bolt installation angle also affects the shear strength of the bolted joint in a way that inclined bolts could generate larger axial forces than the perpendicular bolts, which eventually lead to higher shear stiffness of the bolted rock joints [2, 6, 12, 13](Bjurström, 1974; Haas, 1981; Ludvig, 1983;

Grasselli, 2005). The bolted rock joints with higher shear stiffness will reach the ultimate shear resistance at smaller shear displacements. As for the pretension effects, Haas [12](1981) and McHugh and Signer [14](1999) indicated that pretension loads have little impacts on the shear behaviours of bolted rock joints, which, however contradict the experimental findings of Jalalifar and Aziz [8](2010b), i.e. pretensions could increase the shear stiffness of the bolted joints and result in larger shear loads.

In addition to the above experimental studies, numerical and analytical methods have been used in the studies of bolted rock joints. Haile [15](1999) numerically examined the contributing factors such as bolt diameter, bolt steel types, and bolt inclination angles. Grasselli [6](2005) conducted numerical modelling on double shear tests using FEM code (ZSOIL_3D). Double shear test is a type of test setup for studying the shear behaviours of bolted rock joints. Jalalifar and Aziz [8](2010b) used FEM code ANSYS to study the shear responses of double shear tests. Li et al. [16](2016a) carried out numerical studies on influencing factors using FLAC3D and they concluded that the shear strength of bolted joints are affected by bolt installation angle, bolt diameter and concrete strength. Bahrani and Hadjigeorgiou [17](2017) numerically studied the shear behaviours of bolted rock joints using the reinforcement elements in UDEC. They found that in comparison to "Rock bolt" elements, "Cable" elements underestimate the shear strength of the bolted rock joint. These numerical analyses provide a useful tool to better understand the shear behaviours of bolted rock joints and to examine the contributing factors, as sometimes it is not easy or feasible to conduct large-scale laboratory shear tests on bolted rock joints.

Although many analytical models are proposed to describe the mechanical responses of bolted rock joints subjected to shear loads, most of them focus on the dowel shear loads developed in the bolts and very few could successfully predict the axial forces developed in the bolts. Maekawa and

Qureshi [18](1996) proposed an analytical model in which axial pull-out loads are considered. However, the axial loads in their model do not contribute to the global shear loads, so the global shear loads of the bolted rock joints are simplified to be the dowel shear loads of bolts. Their model is further extended by Soltani and Maekawa [19](2008) and Moradi et al. [20](2012) to path-dependent cyclic loading case. Ma et al. [21](2018) proposed an analytical model for bolts installed perpendicularly to the rock joints, in which the axial loads of bolts are not considered.

Ferrero [5](1995) presented an analytical model to predict the shear strength of rock joint reinforced by rock bolts. In his model, the global shear resistances of the bolted rock joints are associated with two types of forces: the axial forces developed in the bolt due to the shearing movement which become the normal forces acting on the rock joints; and the dowel shear forces acting transversely to the bolt axial direction. However, Ferrero [5](1995)'s model is not able to produce the complete shear load vs shear displacement curve. Furthermore, the factors such as the pretension effects, the bolt installation angle and the interfacial bonding characteristics are not accounted for. Li et al. [22](2015) proposed an analytical model for bolted rock joints, which is able to estimate the ultimate shear strength and joint shear displacement for double shear tests. But, their model also lacks the capacity of predicting the complete curve of the bolt contribution.

Pellet and Egger [10](1996) proposed an analytical model to simulate the shear behaviours of a bolted rock joint when subjected to shearing loads. Similar to Ferrero[5](1995)'s model, the global shear loads in the model of Pellet and Egger[10] (1996) are also attributed to the combination of two effects: the axial forces and dowel shear forces developed in the bolts. The model of Pellet and Egger[10] (1996) could give the complete shear load vs shear displacement curve of bolted rock joints. However, the interfacial bond stress between the bolt and grout is ignored in their model, and the pretension effect is not included in their model. The axial displacement is small for bolts installed

perpendicularly to the rock joints. Pellet and Egger[10] (1996)'s model only accounts for the axial displacement after bolt yielding for perpendicular rock bolts and does not consider the axial displacement prior to the bolt yielding.

A comprehensive analytical model is proposed in this paper to overcome these limitations, by taking into account the axial forces developed in the bolt, the interfacial bond stress between the bolt and grout, the pretension, and the dowel shear forces acting transversely to the bolt axis. In addition, the axial displacement of bolts installed perpendicularly to the rock joint is considered from the beginning of the loading stage.

For a bolted joint subjected to shear loads, the deformed bolt is shown in Fig. 1. Concrete is normally used to represent rock materials in experimental tests. Experimental studies show that two singular points were formed on the bolt: the intersection point O between the bolt and the joint at which the curvature of the deformed bolt is zero and the bending moment is zero; and the point A at which the shear force is zero and the bending moment reaches the maximum value. In addition to the dowel shear forces, the axial forces will be generated in the bolt when the bolt is pulled towards the joint interface during the shearing movement. Consequently, two types of forces are generated in the bolt at the intersection point between the bolt and the joint: the tensile force N_o along the bolt axial direction and the dowel shear force Q_o acting transversely to the bolt, as shown in Fig. 1c. The resultant force of these two forces is R_o in Fig. 1c, which is further decomposed into two forces: R_{ot} and R_{on}. Based on the Mohr-Coulomb criterion, the following formula can be used to compute the global shear force of the bolted rock joint:

$$T_b = R_{ot} + R_{on} tan\emptyset_j \quad (1)$$

where: T_b is the global shear force of a bolted rock joint; R_{ot} is the force component parallel to the rock joint; R_{on} is the force component normal to the rock joint; $\emptyset_j$ is the friction angle of the rock

joint. The cohesion of the rock joint is small in comparison to the forces provided by the bolt and hence is ignored in this study.

Both the axial force N_o and the dowel shear force Q_o are functions of shear displacements. The analytical formulas proposed for N_o and Q_o are presented in Section 2 and 3, respectively.

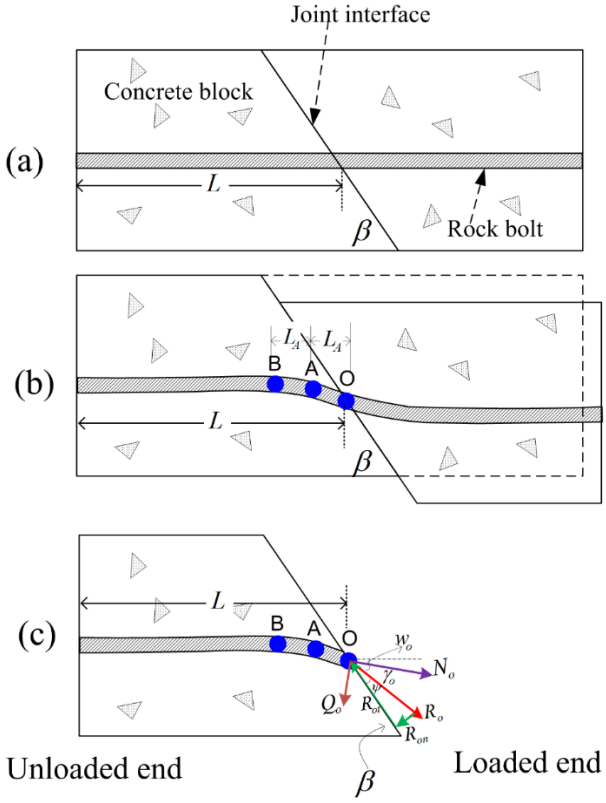

Fig. 1 Deformation of rock bolts when subjected to shear loads. (a) Bolted joint before shearing; (b) Deformed bolt in the two joint blocks; (c) Forces developed in the bolt.

2. Axial load development in bolts with plates

As discussed in section 1, axial loads are mobilized in bolts when bolts are pulled towards the joint interface due to the shearing movement. The following formulas are proposed to predict the axial force evolutions of bolts. In the civil and mining engineering practices, plates and pretension forces

are generally applied at the bolt collar end (i.e. unloaded end in Fig. 1) to improve the bolt's reinforcement capacity. The proposed formulas take into account the effects of the plate and the pretension forces. The bolt installed in one rock block with the length of L (see Fig. 1) is divided into three sections: OA, AB and BC as shown in Fig. 2. The point O is the intersection point; the point A is the hinge point where the moment has the maximum value and the shear force is zero; and the point B is located between points A and C with $L_{AB} = L_{OA} = L_A$.

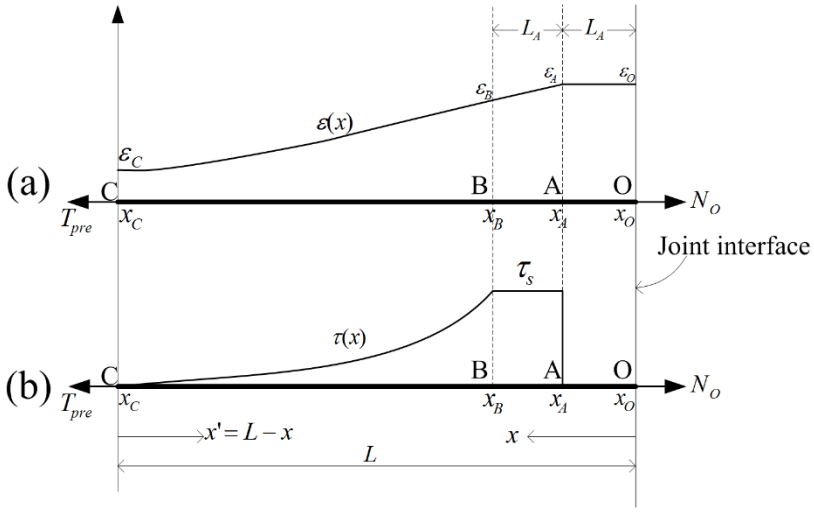

Fig. 2 The strain distribution and the interfacial shear stress distribution along the length of the bolt. (a) Strain distribution; (b) the interfacial shear stress distribution.

With reference to Fig. 2, for OA section, due to the crushing and damage of the grout, the interfacial shear stress is assumed to be zero:

$$\tau(x) = 0 \tag{2}$$

and axial stress is hence expressed as:

$$\sigma(x) = \sigma_o \tag{3}$$

where σ_o is the axial stress of the bolt at section AB.

For AB section, the grout is only partially damaged and the mechanical interlocks between bolt and grout still exist. Hence, the bolt is assumed to have constant interfacial shear stress:

$$\tau(x) = \tau_s \tag{4}$$

and axial stress are expressed as:

$$\sigma(x) = \sigma_o - \frac{\pi d_b}{A}\tau_s(x - x_A) \tag{5}$$

where d_b is the bolt diameter; A is the cross-sectional area of the bolt.

For BC section, the grout is not damaged by the shearing. According to the studies of the Li and Stillburg[23] (1999), Martin et al.[24] (2011) and Ma et al.[25] (2013), the interfacial shear stress can be expressed as:

$$\tau(x) = \tau_s e^{-2\alpha\frac{x-x_B}{d_b}} \tag{6}$$

where α is a coefficient associated with the grout properties, the rock mass and the confining stresses; τ_s is the interfacial shear stress at point B.

The axial stress of the bolt for the BC section can be expressed as:

$$\sigma(x) = \sigma_B - \frac{\pi d_b}{A}\int_{x_B}^{x}\tau(x)\,dx \tag{7a}$$

Substituting Eq. (6) into Eq. (7a) leads to:

$$\sigma(x) = \sigma_B - \frac{\pi d_b \tau_s}{A}\frac{d_b}{2\alpha}\left(1 - e^{-2\alpha\frac{x-x_B}{d_b}}\right) \tag{7b}$$

where, $\sigma_B = \sigma_o - \frac{\pi d_b}{A}\tau_s(x_B - x_A)$ (7c)

At the point C, there is no relative displacement between the bolt and the host concrete as the unloaded end is fixed by the plates. Hence, the interfacial shear stress at point C is equal to zero, i.e. $\tau(L) = 0$, which gives:

$$-2\alpha\frac{L-x_B}{d_b} \approx -10 \tag{8a}$$

and furthermore, the coefficient α can be expressed as:

$$\alpha = \frac{5d_b}{L - x_B} \tag{8b}$$

At the point C, the axial stress of the bolt is:

$$\sigma(\mathrm{L}) = \frac{N_C}{A} \tag{9a}$$

where N_C is the total axial force of the bolt at the point C; N_C is composed of two components:

$$N_C = T_{pre} + N_{aC} \tag{9b}$$

where T_{pre} is the applied pretension force; N_{aC} is the axial force mobilized at point C due to the bolt slip in the axial direction and can be computed by Eq. (7b):

$$\frac{N_{aC}}{A} = \sigma_B - \frac{\pi d_b \tau_s}{A} \frac{d_b}{2\alpha} \left(1 - e^{-2\alpha \frac{x - x_B}{d_b}}\right) \tag{9c}$$

Substitution of Eq. (9c) into Eq. (9b) gives the total axial force mobilized in the bolt at point C:

$$N_C = T_{pre} + \mathrm{N}_o - \pi d_b \tau_s (x_B - x_A) - \frac{\pi d_b^2 \tau_s}{2\alpha} \left(1 - e^{-2\alpha \frac{x - x_B}{d_b}}\right) \tag{9d}$$

where N_o is the axial force of the bolt at the point O.

The axial slip of the bolt at point O is equal to the integration of strain along the bolt and the slip of the unloaded end:

$$S(x') = \int_{x'_C}^{x'_O} \varepsilon(x)\, dx' + S_{un} \tag{10a}$$

where: $x' = L - x$, as shown in Fig. 2; the axial slip of the bolt at the unloaded end is equal to zero, $S_{un} = 0$, because a plate is used and the unloaded end is restrained from moving.

The axial slip of the bolt at the point O can be expressed as:

$$u_o = \int_{x'_C}^{x'_B} \varepsilon(x)\, dx' + \int_{x'_B}^{x'_A} \varepsilon(x)\, dx' + \int_{x'_A}^{x'_O} \varepsilon(x)\, dx' \tag{10b}$$

The strain distributions of the bolt for sections BC, AB and OA can be computed based on the Young's modulus of the bolt and the axial stress distributions expressed by Eqs. (3), (5) and (7b). This implies that the derived equations are only applicable to the bolt in elastic stage.

The computed axial slip is:

$$u_o = \left(\varepsilon_B - \frac{\pi\tau_s d_b^2}{2\alpha AE}\right)(x'_B - x'_C) + \frac{\pi\tau_s d_b^3}{4\alpha^2 AE}\left(1 - e^{-2\alpha\frac{x'_B - x'_C}{d_b}}\right) + \left[\varepsilon_O - \frac{\pi d_b\tau_s}{AE}(L - x_A)\right](x'_A - x'_B) +$$

$$\frac{\pi d_b\tau_s}{AE}\frac{x'^2_A - x'^2_B}{2} + \varepsilon_O(x'_O - x'_A) \quad (10c)$$

where E is the Young's modulus of the bolt.

Substitution of $\varepsilon_O = \frac{N_o}{AE}$ and $\varepsilon_B = \varepsilon_O - \frac{\pi d_b\tau_s}{AE}(x_B - x_A)$ into Eq. (10c) leads to

$$u_o = \frac{N_o}{AE}(x'_O - x'_C) + \left[-\frac{\pi d_b\tau_s}{AE}(x_B - x_A) - \frac{\pi\tau_s d_b^2}{2\alpha AE}\right](x'_B - x'_C) + \frac{\pi\tau_s d_b^3}{4\alpha^2 AE}\left(1 - e^{-2\alpha\frac{x'_B - x'_C}{d_b}}\right) +$$

$$\left[-\frac{\pi d_b\tau_s}{AE}(L - x_A)\right](x'_A - x'_B) + \frac{\pi d_b\tau_s}{AE}\frac{x'^2_A - x'^2_B}{2} \quad (10d)$$

Rearrangement of Eq. (10d) leads to:

$$N_o = \frac{1}{L}(AEu_o + \tau_s H) \quad (10e)$$

where $H = \left[\pi d_b(x_B - x_A) + \frac{\pi d_b^2}{2\alpha}\right](x'_B - x'_C) - \frac{\pi d_b^3}{4\alpha^2}\left(1 - e^{-2\alpha\frac{x'_B - x'_C}{d_b}}\right) + \pi d_b(L - x_A)(x'_A -$

$x'_B) - \pi d_b\frac{x'^2_A - x'^2_B}{2}$ and $\mathrm{L} = x'_O - x'_C$

The interfacial bond stress of fully grouted rock bolts can be computed by the simplified trilinear bond-slip model[24, 26] (Martin et al. 2011; Ma et al. 2016). Fig. 3 shows the trilinear bond-slip model of fully grouted rock bolts. According to the studies of Martin et al.[24] (2011) and Ma et al.[26] (2016), the slip S_1 at which the interfacial shear stress is peaked, usually has a value of a few millimetres. According to double shear tests of Jalalifar[27] (2006), the axial slip u_A would be smaller than S_1 when plates and pretensions are applied at the unloaded end. Hence, the interfacial shear bond stress τ_s can be simply expressed by:

$$\tau_s = k_1 u_A \quad (11a)$$

where k_1 is the stiffness of the bond-slip model in the first stage as shown in Fig. 3; u_A is the slip of the bolt at point A and is computed by:

$$u_A = u_O - \varepsilon_O L_A \tag{11b}$$

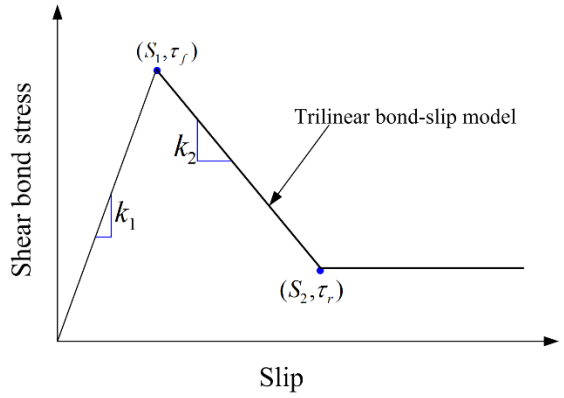

Fig. 3 Trilinear interfacial bond-slip model

Substitution of $\varepsilon_O = \frac{N_o}{AE}$ and Eqs. (11a) and (11b) into Eq. (10e) leads to

$$N_o = \frac{AE + k_1 H}{L + \frac{k_1 L_A H}{AE}} u_o \tag{12}$$

Eq. (12) can be used to calculate the axial force of the bolt at the intersection point O when the bolt is in the elastic stage.

3. The dowel shear behavior of the bolts

When the bolted joint is subjected to shearing, the shear loads are counteracted by the crossing bolt. Dowel action is defined as the counteraction of a bolt to the shear displacement. The dowel shear force is referred as the capacity of the bolt to transfer loads perpendicular to the bolt axis. The dowel shear behaviors of the bolts can be described by the Beam on Elastic Foundation analogy (BEF) theory[10, 18, 21] (Maekawa and Qureshi, 1996; Pellet and Egger, 1996; Ma et al., 2018). In this study, the BEF theory is also used to predict the dowel shear loads of the bolt. In the

BEF theory, the bolt is treated as a semi-infinite beam resting on an elastic foundation and the surrounding concrete is considered as elastic foundation which is represented by springs as show in Fig. 4.

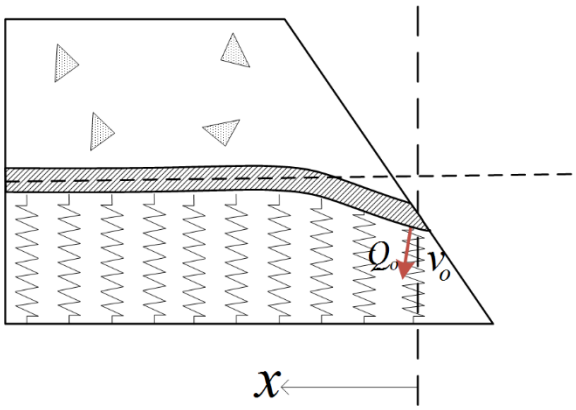

Fig. 4 The dowel shear behavior simulation by the BEF theory.

The differential equation for the BEF system can be expressed as[28] (Timoshenko and Lessels, 1925):

$$EI_b \frac{d^4v}{dx^4} = -kv \tag{13}$$

where *k* refers to the modulus of the elastic foundation (i.e. the spring stiffness); *v* is the transversal displacement of the bolt; E denotes Young's modulus of the bolt; I_b refers to the moment of the inertia of the bolt, which is computed by:

$$I_b = \frac{\pi {d_b}^4}{64} \tag{14}$$

where d_b is the bolt diameter.

The transversal displacement distribution is expressed by:

$$v(x) = \frac{2\lambda \mathrm{Q}_o\, e^{-\lambda x} \cos \lambda x}{k} \tag{15}$$

where Q_o is the dowel shear load applied on the bolt at the intersection point O; and

$$\lambda = \sqrt[4]{\frac{k}{4EI_b}} \quad (16)$$

The slope of the transversal displacement curve can be obtained by differentiating Eq. (15) with respect to *x*:

$$\mathrm{w}(x) = -\frac{2\lambda^2 \mathrm{Q}_o\, e^{-\lambda x}(\cos\lambda x + \sin\lambda x)}{k} \quad (17)$$

The slope angle at the intersection point O is expressed as:

$$\mathrm{w}_o = -\frac{2\lambda^2 \mathrm{Q}_o}{k} \quad (18)$$

The relationship between the dowel shear force Q_o and transversal displacement v_o at the point O is expressed by:

$$\mathrm{Q}_o = \frac{k}{2\lambda}\mathrm{v}_o \quad (19)$$

where v_o is the local transversal displacement of the bolt at $x = 0$.

The local displacement v_o is treated as an input during the analytical analysis and the incremental form of the Eq. (19) is used:

$$d\mathrm{Q}_o = \frac{k}{2\lambda}\mathrm{dv}_o \quad (20)$$

It can be seen from Eq. (20) that the dowel shear force is directly associated with the mechanical properties of the host concrete (the spring stiffness *k*), and the bolt properties (λ: E and I_b). The foundation stiffness *k* recommended in the literature[20, 29-31] (Marcus 1951; Soroushian et al. 1987; Dei Poli et al. 1992; Moradi et al. 2012) produces very scattered values. The formula proposed by Moradi et al.[20] (2012) is used in this paper:

$$k(\Delta) = a \cdot f_c'^{0.85} \quad (21)$$

where f_c' is the compressive strength of the host concrete; a is a coefficient depending upon the test setup and the testing conditions.

With the increasing shear force, the local crushing occurs in the concrete nearby the joint and the host concrete transforms from the elastic stage to the plastic stage. This stage is referred as the ealsto-plastic stage, during which the spring stiffness *k* should be gradually decreased so as to capture the damages in concrete nearby the joint. The stiffness changes can be computed by (modified from Moradi et al.[20]):

$$k(\mathrm{v}) = \frac{a \cdot f_c'^{0.85}}{[1+3(DI(\mathrm{v})-b)^{0.8}]^4} \tag{22}$$

where $DI(\mathrm{v})$ is a non-dimensional damage index.

The damage index *DI* is defined as,

$$DI(\mathrm{v}) = \frac{\mathrm{v}_o}{d_b} \tag{23}$$

The parameter *b* in Eq. (22) is defined as:

$$\mathrm{b} = \frac{\mathrm{v}_{o1}}{d_b} \tag{24}$$

where v_{o1} is the displacement at the beginning point of the elasto-plastic stage as shown in Fig. 5.

Jalalifar and Aziz[8] (2010b) carried out double shear tests on rock bolts. They found that a typical shear load-displacement curve comprises three stages: elastic stage, elasto-plastic stage and plastic stage, as shown in Fig. 5. Ma et al.[21] (2018) have extended the formulas of Maekawa and Qureshi[18] to include three loading stages for bolts installed perpendicularly to the rock joint. During the initial loading stage, the surrounding concrete deform elastically, corresponding to the first stage in Fig. 5. The stiffness *k* remains constant and can be computed by Eq. (21). The gradual decrease

of the foundation stiffness in the elasto-plastic stage can be described by Eq. (22). In the plastic stage, the foundation stiffness is assumed to reach a residual value and remains constant afterwards:

$$k(\Delta) = \frac{a \cdot f_c'^{0.85}}{[1+3(c-b)^{0.8}]^4} \tag{25}$$

$$c = \frac{v_{o2}}{d_b} \tag{26}$$

where v_{o2} is the transversal displacement at the beginning point of the plastic stage as shown in Fig. 5.

The determination of v_{o1}, and v_{o2} will be discussed in the following. It should be noted that, the typical shear load-displacement curve of Jalalifar and Aziz[8] (2010b) is originally the relationship for the global shear loads and the shear displacement. In this study, it is assumed that the dowel shear load vs the shear displacement also exhibit the similar features as the global shear load-displacement curve. This assumption will be justified in the verification part of the paper.

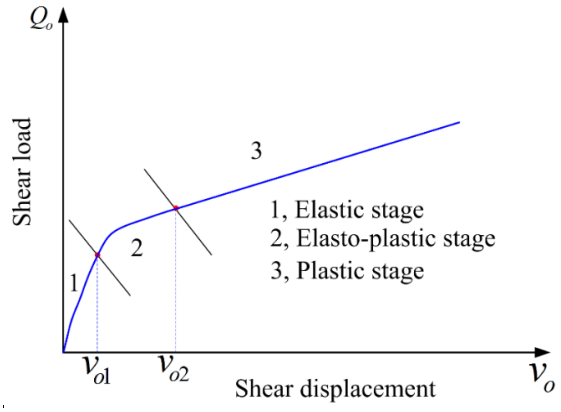

Fig. 5 Typical shear load-displacement curve of double shear tests.

4. Yielding and failure criteria

4.1 Yielding criteria

As the bolt is axially and transversely loaded by the axial force, the shear force, and the bending moment, the yield strain ε_y is not the same as that of the bolt under pure tensile loads. Pellet and Egger[10] (1996) experimentally found that the bolt is first yielded at the hinge point A at which the maximum bending moment is reached. The elastic limit of the rock bolt at the hinge point A can be expressed as[10] (Pellet and Egger, 1996):

$$\sigma_y = \frac{M_A}{W_b} + \frac{N_A}{A} \tag{27}$$

where W_b is section modulus and $W_b = \frac{\pi {d_b}^3}{32}$

The bending moment M_A at point A is proposed by Pellet and Egger[10] (1996) based on the moment equilibrium at A as shown in Fig. 6:

$$M_A = \frac{\mathrm{Q}_o^2}{2p_u} \tag{28}$$

where p_u is the maximum pressure of the reaction force per unite length.

Considering the forces acting perpendicularly to the bar axis, the following force equilibrium can be reached.

$$\mathrm{Q}_o = p_u L_A \tag{29a}$$

From this equation, the length of L_A can be computed by:

$$L_A = \frac{\mathrm{Q}_o}{p_u} \tag{29b}$$

The maximum pressure p_u can be associated with the compressive strength of the host material and be computed by Ferrero[5], 1995):

$$p_u = \mu f_c' d_b \tag{30}$$

where f_c' is the compressive strength of the host concrete; d_b is the diameter of the bolt; μ is a factor that depends on the rock properties and $\mu \geq 1$.

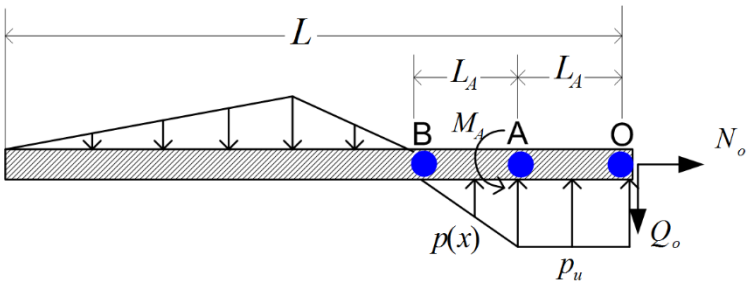

Fig. 6 The simplified loading on the bolt, after Pellet and Egger[10] (1996)

Substitution of Eq. (28) into Eq. (27) leads to

$$N_A = \sigma_y A - \frac{A Q_o^2}{2 p_u W_b} \tag{31}$$

Eq. (31) is the elastic limit of the bolt at the hinge point A.

4.2 Failure criteria

Theoretically, the bolt failure could occur at the intersection point O and also could occur at the hinge point A. However, according to the studies of Pellet and Egger[10] (1996) and Jalalifar and Aziz[8] (2010b), the bolts tend to break at the intersection point O under the interaction of the axial and shear forces. Hence, in this study, only the failure at the intersection point O will be discussed. Two failure criteria are presented herein to predict the failure status of bolts.

First failure criteria

The failure criteria for rock bolts at the intersection point O is caused by the combined action of the axial force N_o and the shear force Q_o[32]:

$$\left(\frac{N_o}{N_p}\right)^2 + \left(\frac{Q_o}{Q_p}\right)^2 = 1 \tag{32}$$

where, N_p and Q_p represent the corresponding ultimate axial force and shear force under non-interactive force conditions, respectively; $N_p = A\sigma_p$; $Q_p = \frac{A\sigma_p}{\sqrt{3}}$ (Von-Mises criteria); σ_p is the ultimate axial stress at failure.

Second failure criteria

Maekawa and Qureshi[18] (1996) suggested a failure function for dowel bars:

$$\left(\frac{M_o}{M_p}+\left(\frac{N_o}{N_p}\right)^2\right)^2+\left(\frac{Q_o}{Q_p}\right)^2=1 \quad (33)$$

where: M_p is the value of bending moment when $M_p=\frac{\sigma_p D^3}{6}$.

At the intersection point, $M_o=0$ and hence Eq. (33) becomes:

$$\left(\frac{N_o}{N_p}\right)^4+\left(\frac{Q_o}{Q_p}\right)^2=1 \quad (34)$$

Fig. 7 shows a typical stress-strain relationship of the steel rebar under tension. This tensile stress-strain curve comprises three stages: elastic stage, yield plateau and hardening stage. The axial stress of a bolt increases linearly at a slope of E prior to reaching the yield strength σ_y. This is followed by a yield plateau, where the axial stress remains at σ_y when the strain is between ε_y and ε_{sh}. Afterwards, the axial stress increases linearly at a smaller slope of E_r and this stage is referred as the hardening stage. In Fig. 7, ε_y denotes the bolt yield strain and ε_{sh} denotes the strain at the onset of hardening phase. The yield plateau stage in Fig. 7 is accounted for in this study and is presented in Section 5.

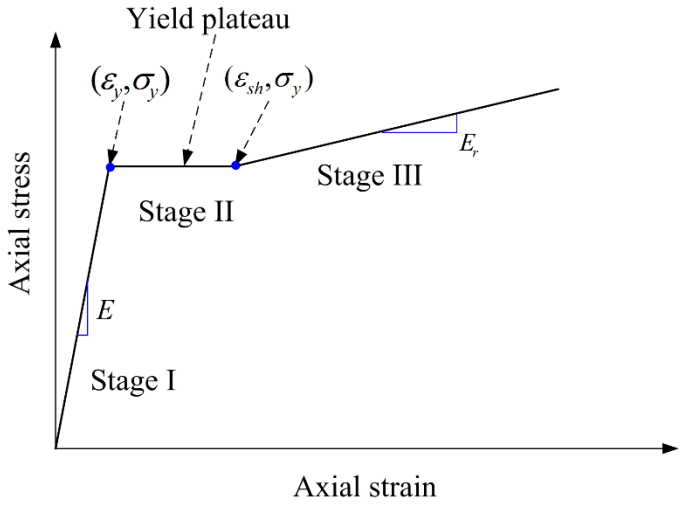

Fig. 7 The axial behavior of bolts under tension.

The yielding and failure mechanism of the bolt material is considered in Pellet and Egger[10] (1996) and the crushing and damage of the concrete is taken into account in Maekawa and Qureshi[18] (1996). However, the mechanical responses of these two materials, i.e. bolts and concrete, are not considered simultaneously in the previous studies. This study takes into account the mechanical responses of both materials. In Section 3, the foundation stiffness *k* is expressed by three equations, which correspond to three distinct stages in Fig. 5, respectively. It is difficult to experimentally obtain the values of v_{o1}, and v_{o2}, which are normally obtained by curve-fitting technique. As the surrounding concrete and the bolt interact with each other during the shearing process, it is reasonable to assume that these two materials enters into their respective second-stage simultaneously (see Figs. 5 and 7), and similarly, enters into their respective third-stage simultaneously.

In this study, the above assumption is adopted when computing the values of v_{o1}, and v_{o2}, without the assistance of the curve-fitting technique, which enables the proposed model to become more applicable. When the bolt is yielded (by Eq. 31), the bolt material enters into the yield plateau stage in Fig. 7 and the foundation enters into the elasto-plastic stage in Fig. 5. When the axial strain of the bolt grows larger than ε_{sh}, the bolt enters into the hardening stage in Fig. 7 and the foundation enters into the plastic stage in Fig. 5. With the increasing shear loads, the bolt reaches the failure limits and breaks out, which is determined by Eq. (32) or Eq. (34).

5. Axial loads of bolts after yielding

The formulas for axial loads and the dowel shear loads are presented in Sections 2 and 3, respectively. The dowel shear load-displacement curve has three distinct stages as shown in Fig. 5. The proposed formula for the axial load in Section 2 is only applicable for bolts in the elastic stage. The following formula is proposed for the axial loads of bolts after yielding.

The shear displacement increases significantly after the bolt is yielded. It is assumed that the hinge point location remains constant and in the meantime the length of L_A increases with the increasing shear displacement as shown in Fig. 8. This assumption was found reasonable by Pellet and Egger (1996). Based on the geometrical consideration, the following equation which takes into account the large displacement, can be used to correlate the plastic deformation of the bolt and the shear displacement:

$$\frac{\Delta U_{op}(j)}{\sin\left(\Delta w_{op}(j)\right)} = \frac{L_A(j-1)}{\sin\left(\beta - w_o(j-1) - \Delta w_{op}(j)\right)} = \frac{L_A(j)}{\sin\left(\pi - \beta + w_o(j-1)\right)} \tag{35}$$

where $\Delta U_{op}(j)$ is the incremental shear displacement at step j when the bolt is in plastic stage; $L_A(j)$ is the length of the section OA at step j; $w_o(j-1)$ is the accumulated rotation angle of the bolt until step j-1; $\Delta w_{op}(j)$ is the incremental rotation angle of the bolt at step j.

From Eq. (35), the incremental rotation angle can be expressed as:

$$\Delta w_{op}(j) = arctan\left(\frac{\Delta U_{op}(j)\cdot\sin\left(\beta - w_o(j-1)\right)}{L_A(j-1) + \Delta U_{op}(j)\cdot\cos\left(\beta - w_o(j-1)\right)}\right) \tag{36}$$

The accumulated rotation angle of the bolt from the beginning of the loading stage until the step j is computed by:

$$w_o(j) = w_o(j-1) + \Delta w_{op}(j) \tag{37}$$

In the first loading step ($j = 1$) after the bolt yielding, the rotation angle at step $j = 1$ is computed by:

$$w_o(j=1) = w_{oe} + \Delta w_{op}(j=1) \tag{38}$$

where: w_{oe} is the accumulated bolt rotation angle at the end of the bolt elastic stage.

The length of the section OA at step $j = 1$ can be computed by:

$$L_A(j) = \frac{\Delta U_{op}(j) \cdot \sin\left(\pi - \beta + w_o(j-1)\right)}{\sin\left(\Delta w_{op}(j)\right)} \quad (39)$$

The bolt strain at step j can be obtained by:

$$\varepsilon(j) = \frac{L_A(j) - L_A^e}{L_A^e} \quad (40)$$

where L_A^e is the length of the bolt prior to yielding.

When the computed strain is smaller than the strain at the onset of the hardening section, i.e. $\varepsilon(j) < \varepsilon_{sh}$, the axial force of the bolt will remain constant as N_e.

N_e is the axial force of the bolt in the yield plateau and is computed by:

$$N_o(j) = N_e = E\varepsilon_y A \quad (41)$$

When the computed strain $\varepsilon(j) \geq \varepsilon_{sh}$, the axial force of the bolt at the intersection point O is computed by:

$$N_o(j) = N_e + (\varepsilon(j) - \varepsilon_{sh}) \cdot E_m \cdot A \quad (42)$$

where E_m is the Young's modulus of bolt in the hardening stage.

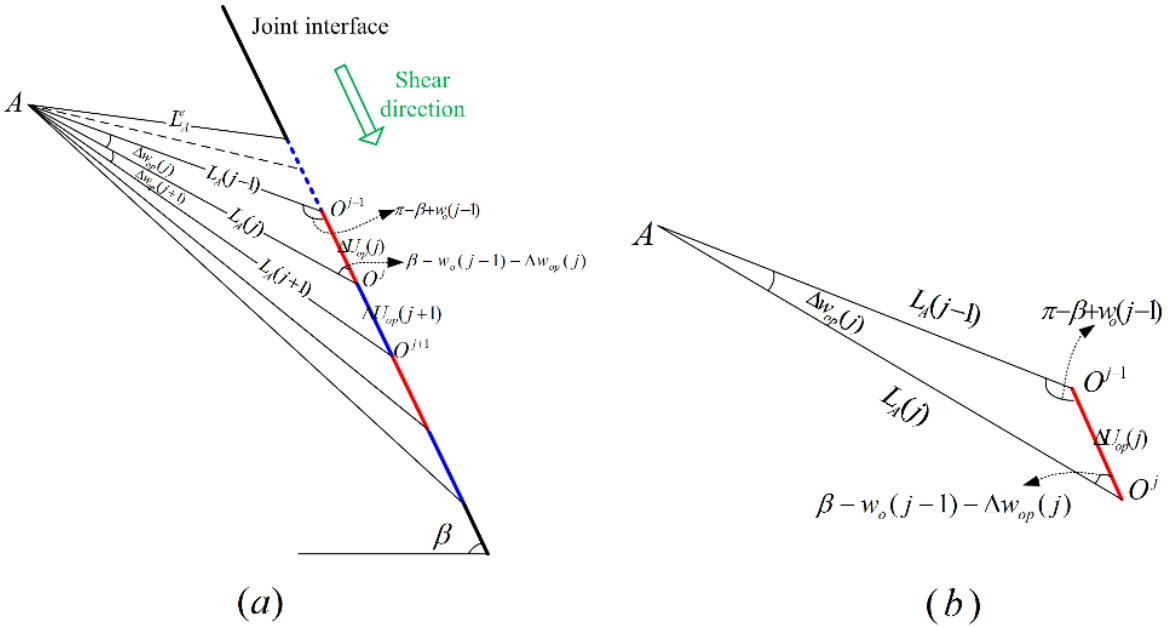

Fig. 8 The large deformation after bolts are yielded. (a) Large deformation of the bolt under various incremental shear displacements; (b) Close-up view of the bolt deformation under the shear displacement of $\Delta U_{op}(j)$.

6. Computational procedure

The global shear displacement U_o is considered as input and is divided into many loading steps ΔU_o. The incremental shear displacement ΔU_o is decomposed into u_o and v_o which is shown in Fig. 9. The axial displacement of the bolt at point O is computed by:

$$u_o = \Delta U_o \cos(\beta - w_o) \tag{43}$$

and the transversal shear displacement is computed by:

$$v_o = \Delta U_o \sin(\beta - w_o) \tag{44}$$

The resultant force of the axial force N_o and the dowel shear force Q_o is computed by:

$$R_o = \sqrt[2]{N_o^2 + Q_o^2} \tag{45}$$

The angle between the resultant force R_o and the axial force N_o as shown in Fig. 10 is computed by:

$$\gamma_o = \tan^{-1}\frac{Q_o}{N_o} \quad (46)$$

The forces parallel and normal to the rock joint are computed by the following equations:

$$R_{ot} = R_o \cos(\beta - w_o - \gamma_o) \quad (47)$$

$$R_{on} = R_o \sin(\beta - w_o - \gamma_o) \quad (48)$$

When pretension effect are considered, the pretension forces can be regarded as the external force applying to the rock joint. Thus, Eq. (1) can be modified as:

$$T_b = (R_{ot} - N_C cos\beta) + (R_{on} + N_C sin\beta) tan\emptyset_j \quad (49)$$

where: N_C is the axial force at the unloaded end of the bolt.

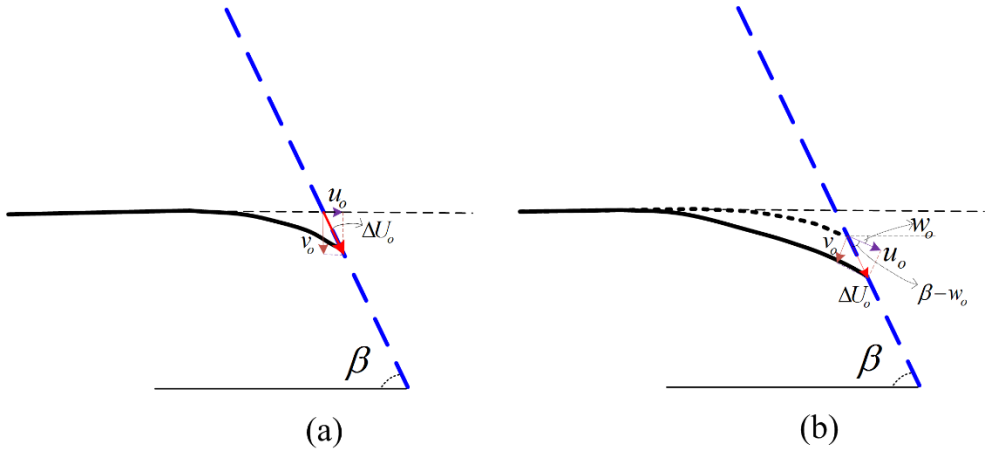

Fig. 9 The decomposition of the incremental global shear displacement ΔU_o. (a) The first incremental shear displacement, $w_o = 0$; (b) The subsequent incremental shear displacement.

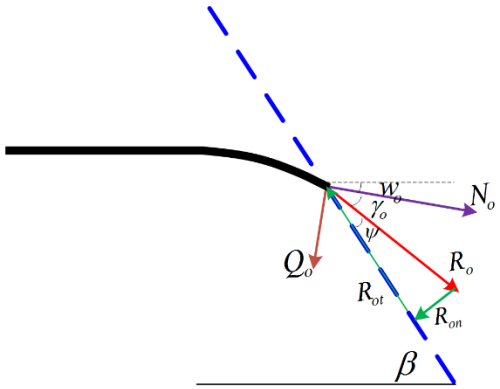

438

439 Fig. 10 The resultant force R_o, and the forces parallel and normal to the rock joint

440 The computational procedure of the proposed model is summarized in Fig. 11.

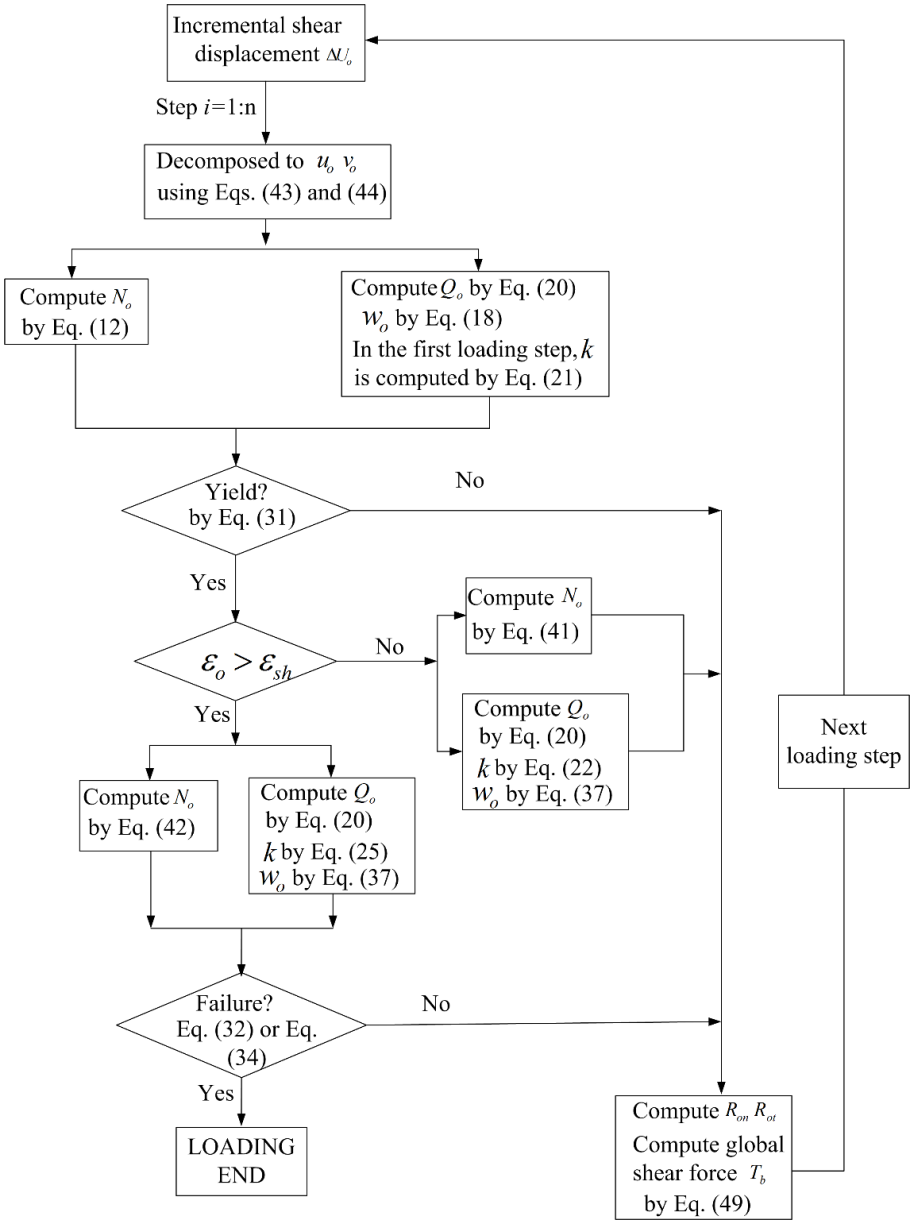

Fig. 11 The computational procedure of the proposed model

7. Model verification

Double shear tests and single shear tests are the two commonly used test setups in examining the shear behaviours of bolted rock joints. Hence, some experimental double shear tests and single shear tests containing the axial load evolution and shear load evolution are used to verify the proposed analytical model.

448 **7.1 Double shear tests**

449 Jalalifar[27] (2006) carried out a series of double shear tests on rock bolts installed in concrete with
450 compressive strength of 20 and 40 MPa, under pretensions of 20 kN, 50 kN and 80 kN. In his tests,
451 except for the global shear loads, the axial force evolution at the unloaded end of the bolt was also
452 recorded. Thus, these data are ideal to verify the proposed axial force evolution model as well as
453 the global shear load model.

454 The setup of the double shear experiment is schematically shown in Fig. 12. Loading cells were
455 installed at the two unloaded ends of bolts and the axial load developments were recorded. It should
456 be noted that the applied load P is equal to two times the shear load T_b computed by Eq. (49), i.e.
457 $P = 2T_b$, as the double shear tests consists of two bolted joints. The shear displacement U_{DST} of
458 the steel block is equal to two times the global shear displacement U_o: $U_{DST} = 2U_o$.

459 The following parameters can be obtained directly from the test setup: $\beta = 90°$, $L = 150$ mm,
460 $D = 21.7$ mm, $f_c' = 20$ and 40 MPa, $T_{pre} = 20, 50\ and\ 80\ kN$, $E = 200$ GPa, $\sigma_y = 680\ MPa$,
461 $\sigma_p = 950\ MPa$. The friction angle of the joint is estimated as: $\emptyset_j = 30°$. The parameter μ in Eq.
462 (30) is selected as: $\mu = 2$; the parameter a in Eq. (21) is chosen as: $a = 2$. In addition, the
463 parameters E_m and ε_{sh} are chosen as: $E_m = 1\ GPa$; and $\varepsilon_{sh} = 0.008$. The stiffness of the
464 interfacial bond-slip model in Fig. 3 is chosen as: $k_1 = 4\ GPa/m$, which is estimated based on the
465 pullout tests of studies of Aziz and Jalalifar[33] (2005).

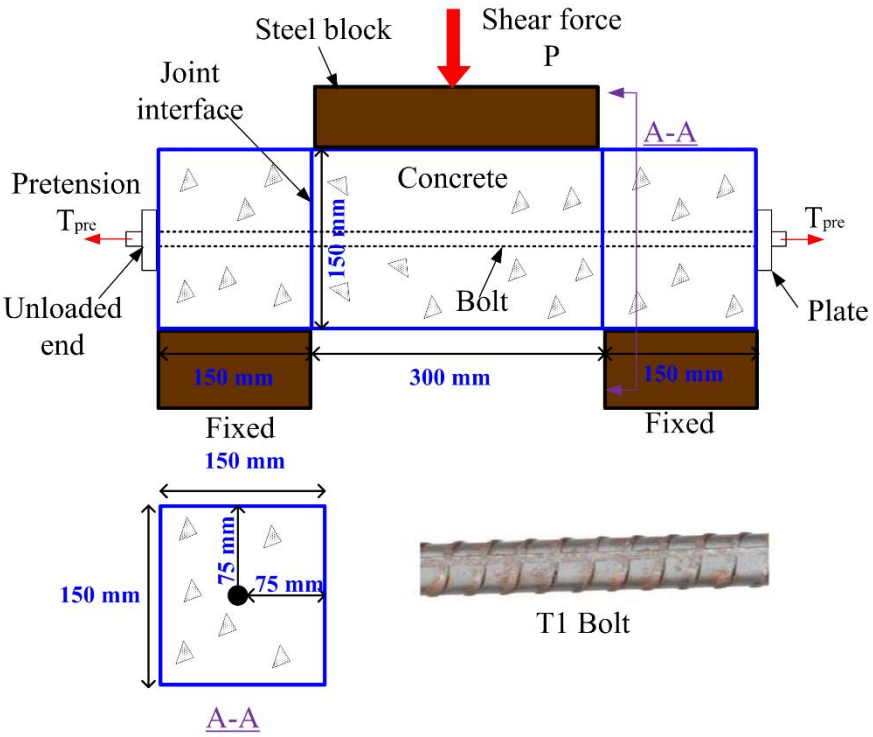

Fig. 12 Test setup of double shear tests

Three types of curves are predicted by the proposed analytical model: axial load at the bolt unloaded end vs the global shear displacement, dowel shear load vs the global shear displacement, the global shear load vs the global shear displacement. Firstly, the shear behaviours of double shear tests with concrete strength of $f_c' = 20$ MPa are modelled under pretension loads 20, 50 and 80 kN, respectively. The predicted curves are shown in Fig. 13. The experimental results of axial load development at the bolt unloaded end and the global shear loads are also shown in the figure. It can be seen that the proposed model is able to predict global shear force development as well as the axial force evolution. Experimental tests did not provide the dowel shear load evolution and thus, the analytical predictions on the dowel shear load are presented in the figure without verification.

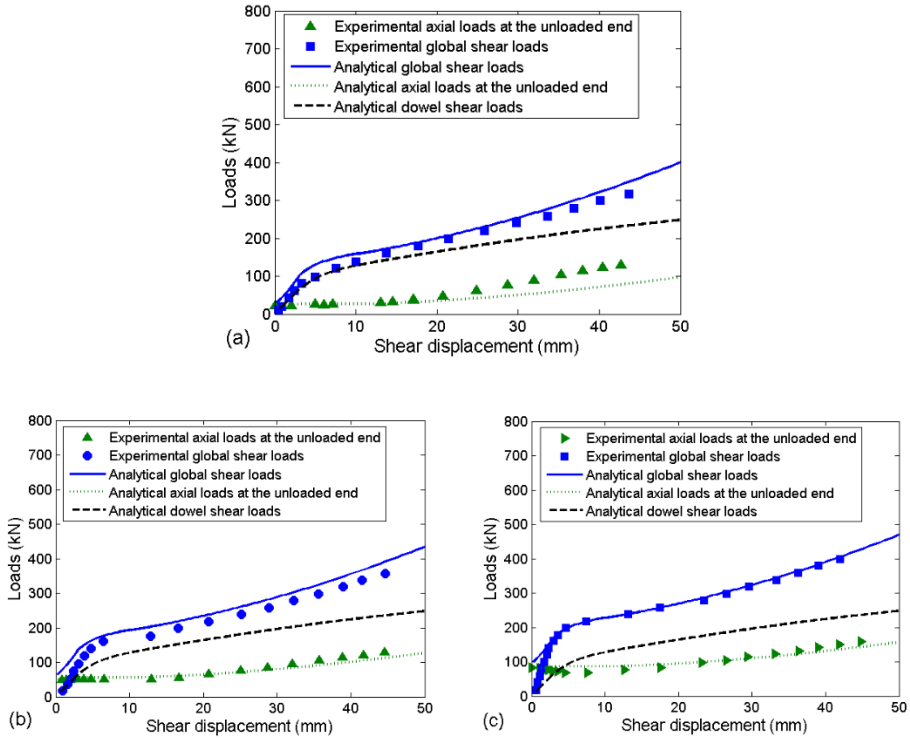

Fig. 13 Comparison between experimental data and the proposed analytical model for bolts installed in concrete with f_c' of 20 MPa. (a) Pretension load of 20 kN; (b) Pretension load of 50 kN; (c) Pretension load of 80 kN.

As discussed in Section 1, many existing models cannot give good predictions on the axial force development, because the interfacial bond stress and the pretension are not considered in these models. The model proposed in this study is able to predict the axial forces in the bolts. The predicted axial forces under three different pretension forces 20, 50 and 80 kN are shown in Fig. 14. Also shown in the figure are the experimental axial force evolutions of bolts under the three pretension forces. The comparison indicates that the proposed model matches well with the experimental axial force evolutions under various pretensions. In addition, it can be concluded that the increasing pretension loads could lead to increased axial forces in the bolt. The axial forces do

not show obvious increase in the first 15 mm shear displacement and afterwards, the axial forces increase gradually.

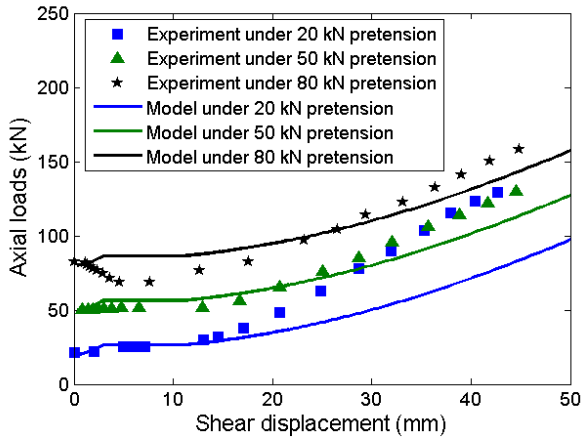

Fig. 14 Axial force evolutions for double shear tests under pretensions of 20, 50 and 80 kN.

Fig. 15 shows comparison of global shear force-shear displacement curves for experiments and the analytical model, under the three different pretension forces. It can be seen that the pretension forces could increase the global shear forces of bolted rock joint. Larger pretension forces result in larger shear forces. The proposed model successfully captures the pretension effects and closely matches the experimental shear load vs displacement curves.

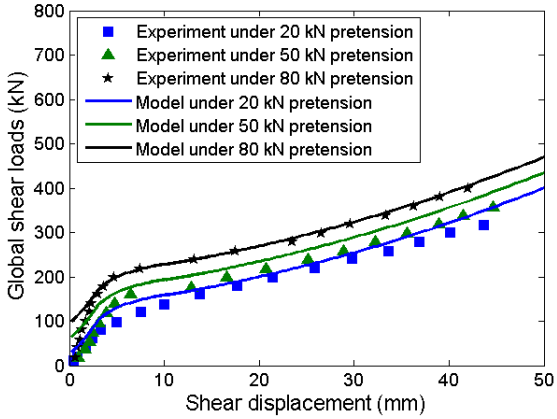

Fig. 15 Global shear force evolutions for double shear tests under pretensions of 20, 50 and 80 kN.

Fig. 16 shows the comparison between experimental data and the proposed model in concrete strength of 40 MPa under pretensions of 20, 50 and 80 kN. It can be seen that the proposed model is still able to predict the axial force evolutions and global shear load evolutions for bolts installed in concrete with higher compressive strength. This indicates that the proposed model accounts for the effect of the concrete strength.

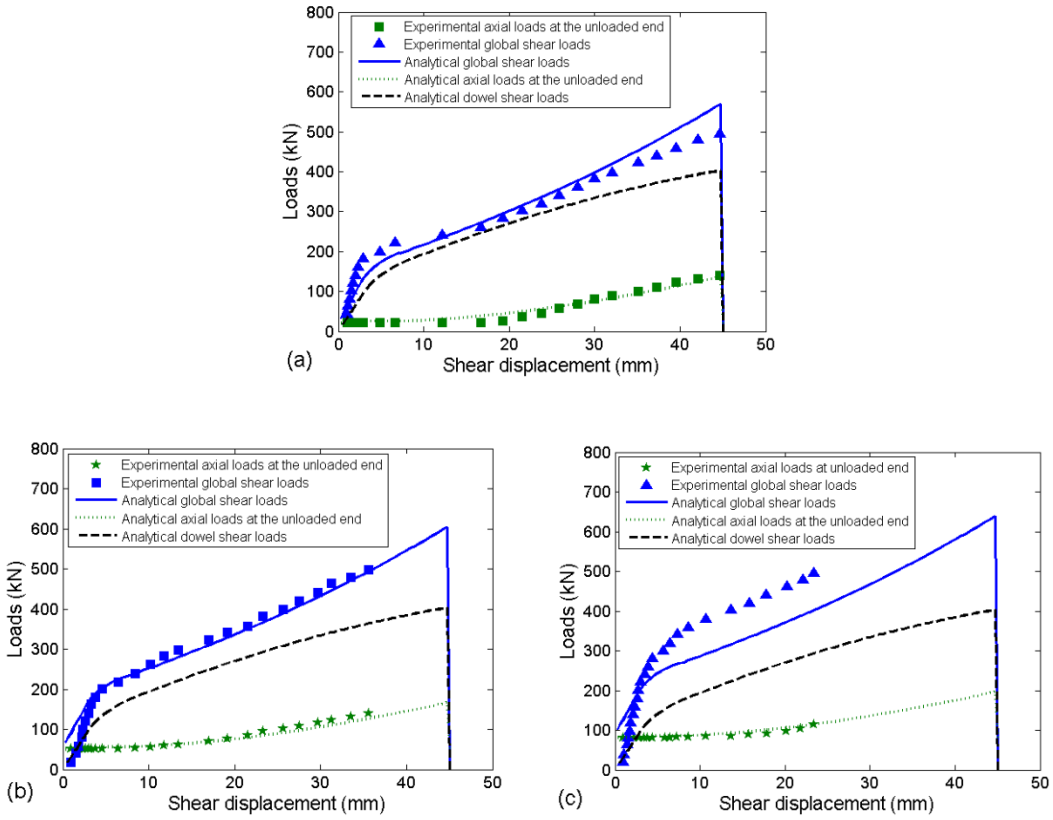

Fig. 16 Comparison between experimental data and the proposed analytical model for bolts installed in concrete with f_c' of 40 MPa. (a) Pretension load of 20 kN; (b) Pretension load of 50 kN; (c) Pretension load of 80 kN.

Fig. 17 shows comparisons of the axial force evolutions of experiments and the proposed model in concrete strength of 40 MPa. Comparing the axial load-displacement curves shown in Figs. 14 and 17 which are obtained under concrete strengths of 20 and 40 MPa, respectively, it can be seen that the stronger concrete leads to higher axial forces. For clarity reasons, the curves in Figs. 14 and 17 are not put together in one single figure.

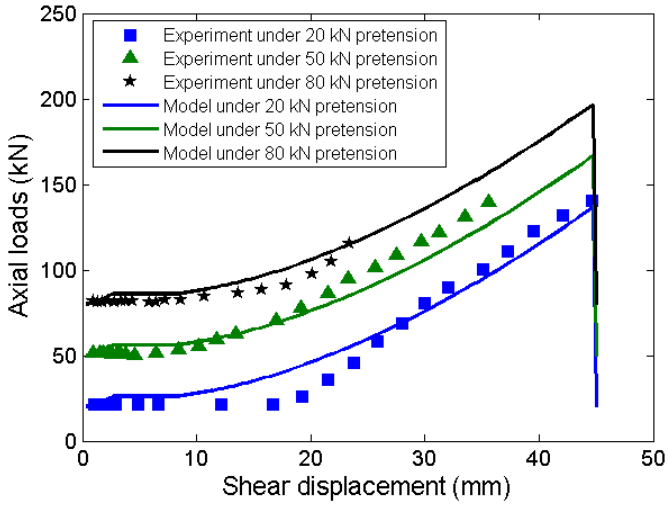

Fig. 17 Axial force evolutions for double shear tests in concrete strength of 40 MPa under pretensions of 20, 50 and 80 kN.

Fig. 18 shows the global shear force evolutions for double shear tests in concrete strength of 40 MPa. Comparing the curves in Fig. 18 with those in Fig. 15, it can be seen that higher concrete strength results in higher global shear force. The proposed model matches well with the shear forces of bolts under pretensions of 20 and 50 kN in Fig. 18 while it underestimates the shear force of the bolt under pretension of 80 kN. This might be caused by the experimental process for bolts under pretension of 80 kN. Nevertheless, the proposed model could predict the global shear force evolutions in a reasonable accuracy.

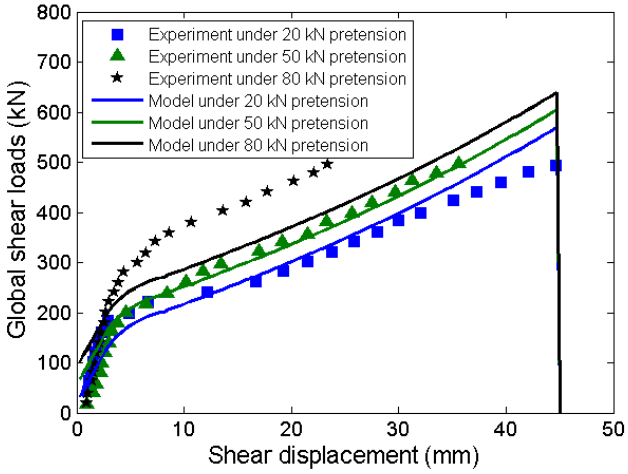

Fig. 18 Global shear force evolutions for double shear tests in concrete strength of 40 MPa under pretensions of 20, 50 and 80 kN.

It can be seen from Fig. 16, the bolts are predicted to fail at the shear displacement of around 45 mm. The double shear tests under pretension of 50 and 80 kN were terminated at around 35 mm and 25 mm, respectively. The bolt in the experiments under pretension force of 20 kN do not fail within 45 mm shear displacement. This implies that the failure criteria have a tendency to under predict the ultimate shear load of the bolts.

Eq. (34) is used as the failure criteria in the above analytical modelling. The relationship between the axial force and the dowel shear force of bolt at point O is shown in Fig. 19, together with two failure criteria Eqs. (32) and (34). It can be seen that Eq. (32) produces a lower ultimate shear load than Eq. (34), and thus Eq. (34) is more suitable to be used as the failure criteria.

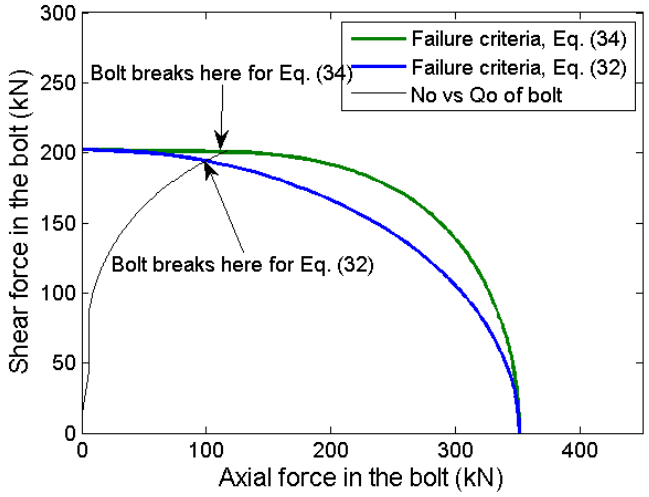

Fig. 19 The failure criteria Eqs. (32) and (34) and the axial force vs the dowel shear force of the bolt at point O

7.2 Single shear test

In the above section, the proposed analytical model is verified by the double shear tests of rock bolts. In the double shear tests, there are two bolted joints and thus, the overall shear load of double shear test is equal to two times the computed T_b. Additionally, a single shear test is used to further verify the analytical model.

Goris et al.[34] (1996) conducted single shear tests on fully grouted cable bolts. The test setup is shown in Fig. 20. One test was conducted on the smooth joint with the friction angle of 30°. The diameter of the cable bolt is 15.24 mm. The compressive strength of the concrete is 68.9 MPa. The encapsulation length of the bolt in the concrete block is 200 mm. The pretension is 0 kN and the axial force of the bolted joint is recorded during the test processing. According to the test setup, the following parameters are determined as: $\beta = 90°$, $L = 200$ mm, $\emptyset_j = 30°$, $f_c' = 68.9$ MPa, $T_{pre} = 0\ kN$. The properties of the cable bolt are estimated as: $E = 200$ GPa, $\sigma_y = 680\ MPa$,

563 $\sigma_p = 1000\,MPa$. The other parameters are selected as: μ = 2, a = 2, $k_1 = 4\,GPa/m$, $E_m =$

564 $1\,GPa$ and $\varepsilon_{sh} = 0.008$, which are the same as those used in the double shear tests.

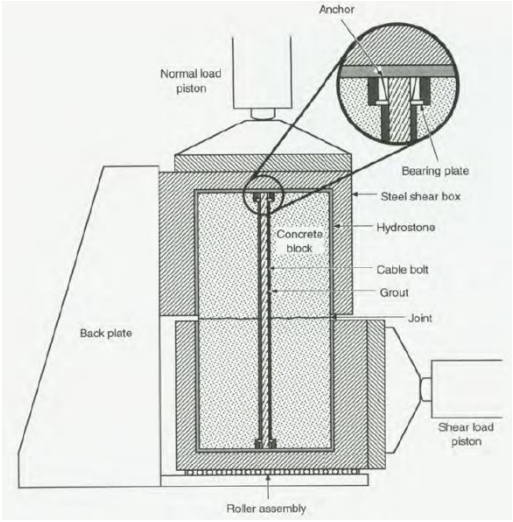

565

566 Fig. 20 The experimental setup of Goris et al.[34] (1996)

567 Fig. 21 shows the comparison between the analytical model and the experimental data. It can be

568 seen that the predicted global shear load evolution and the axial force evolution match well with

569 the experimental data.

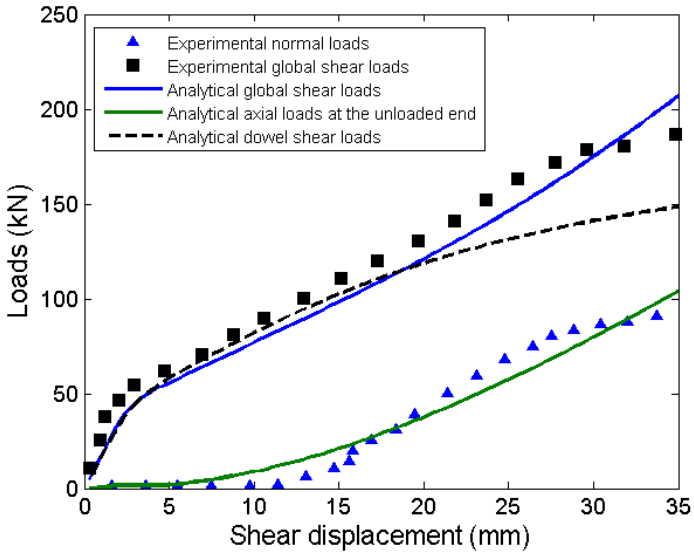

570

Fig. 21 Comparison between experimental data and the proposed analytical model for cable bolt in single shear test of Goris et al.[34] (1996).

8. Effects of the concrete strength f_c', the inclination angle β and the friction angle $\emptyset_j$

From the literature review, it is generally accepted that the pretension, the concrete strength, the bolt inclination angle and the friction angle could significantly affect the shear behaviors of the bolted joint. The effects of the pretension are already discussed and presented in the previous sections. The effects of the concrete strength f_c', the inclination angle β and the friction angle $\emptyset_j$ are investigated herein. The parameters of $L = 150$ mm, $D = 21.7$ mm, $E = 200$ GPa, $\sigma_y = 680\ MPa$, $\sigma_p = 950\ MPa$, $\mu = 2$, $a = 2$, $k_1 = 4\ GPa/m$, $E_m = 1\ GPa$, $\varepsilon_{sh} = 0.008$, are used in the following analytical investigations. These parameters are the same as those used when modelling the double shear tests of Jalalifar[27] (2006). The pretension of $T_{pre} = 50$ kN is used in the modelling. Note that in this section, the shear behaviors of single shear tests are modelled and hence, the obtained global shear load is equal to T_b.

8.1 Effects of the concrete strength f_c'

To examine the effects of the concrete strength, the concrete compressive strength of $f_c' = 20$, 40, 60 and 80 MPa are used in the analytical modelling. Among them, the numerical shear behaviors of bolted rock joints with $f_c' = 20$ and 40 MPa have been verified by the experimental tests of Jalalifar[27] (2006) in Section 7. The bolt inclination angle and the friction angle used in the modelling are $\beta = 90°$ and $\emptyset_j = 30°$, respectively. The obtained global shear load vs shear displacement curves and the axial force vs shear displacement curves for concrete strength of 20, 40, 60 and 80 MPa are shown in Fig. 22. As can be seen, increasing concrete strength could

593 increase the axial loads N_C at the point C and global shear loads T_b. The bolts installed in higher
594 concrete strength fail at smaller shear displacement.
595 Fig. 23 shows the dowel shear loads and axial loads developed in the bolt at the intersection point
596 O. Fig. 24 illustrates the failure envelope and the axial force vs shear force curve of the bolt at the
597 intersection point O under concrete strength of 20, 40, 60 and 80 MPa, respectively. It can be seen
598 from Fig. 23 that larger dowel shear forces are mobilized in higher concrete strength. According
599 to the failure criteria Eq. (34) as shown in Fig. 24, the bolt installed in higher concrete strength
600 fails at larger dowel shear load and smaller axial load. It is worth noting that the bolted joint with
601 higher concrete strength might have smaller ultimate T_b as shown in Fig. 22. This can be explained
602 by the fact that the ultimate axial force N_C of the bolted joint with higher concrete strength is
603 smaller when the bolt breaks out, meaning that the normal force acting on the joint is small, which
604 leads to small global shear load T_b according to Eq. (49) despite the higher dowel shear force.

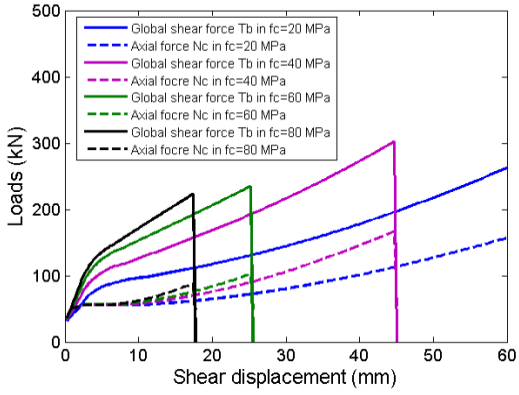

605

606 Fig. 22 The global shear loads T_b and the axial loads N_C in concrete strength of 20, 40, 60 and 80
607 MPa.

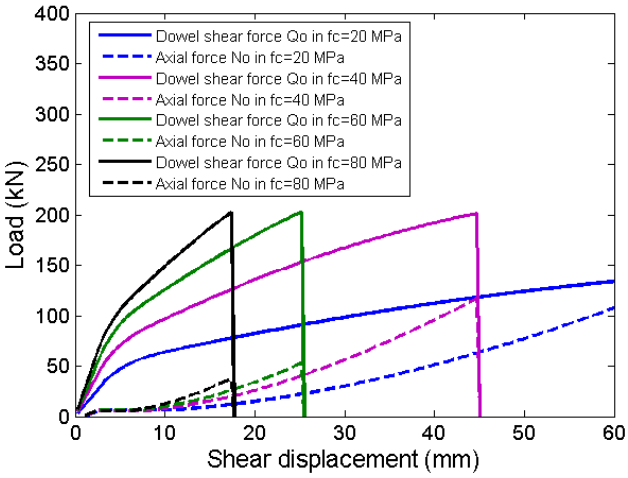

608

609 Fig. 23 The dowel shear loads Q_o and the axial loads N_o at the intersection point O in concrete

610 strength of 20, 40, 60 and 80 MPa.

611

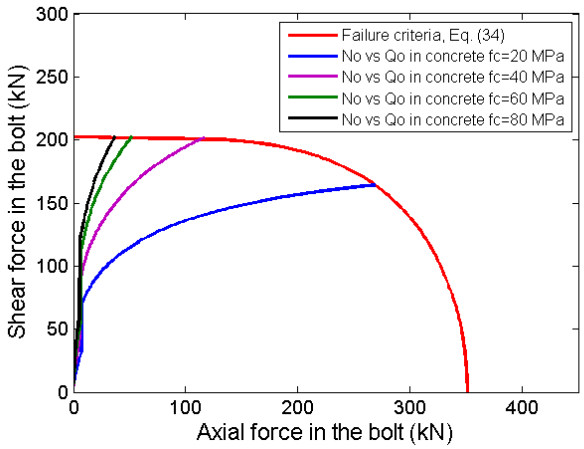

612

613 Fig. 24 The failure criteria Eq. (34) and the axial force vs the dowel shear force of the bolt at the

614 intersection point O in concrete strength of 20, 40, 60 and 80 MPa.

615

616 **8.2 Effects of the inclination angle β**

617 It is difficult to conduct shear tests on inclined bolts, and there are few experimental tests in the

618 literature which contain shear load evolution and axial load evolution of the inclined bolts. Thus,

comparisons between the experiments and the analytical model cannot be carried out, and only the analytical predictions on various inclination angles are presented herein. The concrete compressive strength of $f_c' = 40$ MPa and the friction angle of $\emptyset_j = 30°$ are used when examining the effects of the inclination angle.

Fig. 25 shows the shear load vs shear displacement curves and axial load vs shear displacement curves of bolted rock joints with inclination angles of 90˚, 80˚, 60˚ and 30 ˚. The numerical shear behaviors of bolted rock joints with the inclination angle of 90˚ have been verified by the experimental tests of Jalalifar[27] (2006) in Section 7. It can be seen from Fig. 25 that a smaller inclination angle leads to a larger axial load, which further increase the global shear load. The ultimate shear displacement of bolts decreases with the decreasing inclination angle.

Fig. 26 illustrates the failure envelope and the axial force N_o vs dowel shear force Q_o of bolts at inclination angles of 90˚, 80˚, 60˚ and 30 ˚. In the analytical modelling, Eq. (34) is used as the failure criteria. It can be seen that for smaller inclination angles, the axial loads developed in the bolt contributes significantly to the bolt failure.

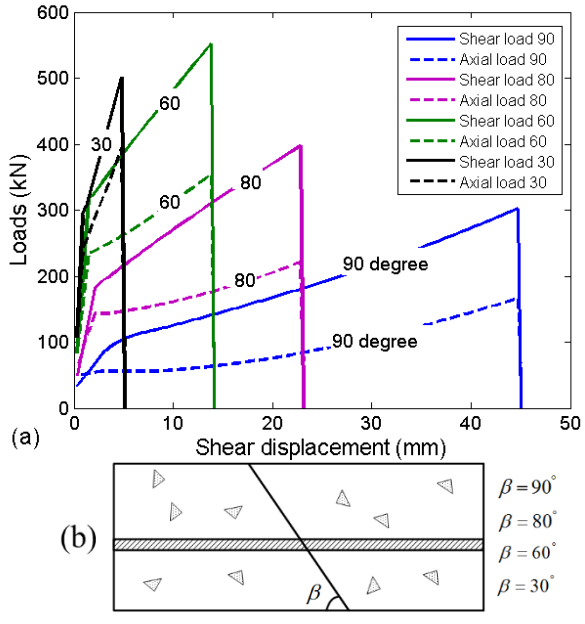

Fig. 25 (a) The global shear load T_b vs shear displacement curves and axial load N_c vs shear displacement curves of bolted rock joints with inclination angles of 90˚, 80˚, 60˚ and 30 ˚; (b) single shear test setup with various angles.

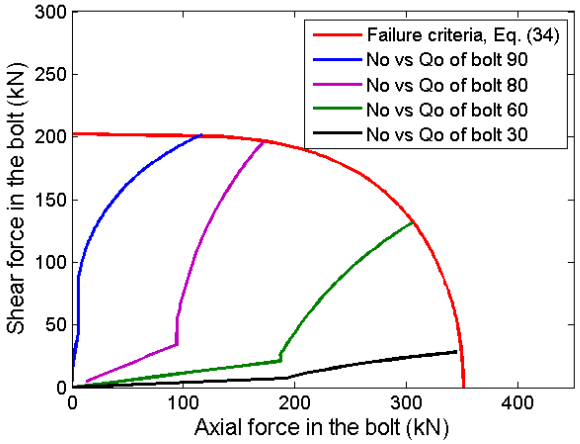

Fig. 26 The failure criteria Eq. (34) and the axial force N_o vs dowel shear force Q_o of the bolt with inclination angles of 90˚, 80˚, 60˚ and 30 ˚.

8.3 Effects of the friction angles $\emptyset_j$

The friction angle of the joints can also affect the shear strength of the bolted rock joints. The effects of the friction angle are investigated herein. The concrete strength of $f_c' = 20$ MPa and the bolt inclination angle of $\beta = 90°$ are used in the analytical modelling. The friction angles of 15˚, 30˚ and 45˚ are examined. Fig. 27 shows the global shear load T_b vs the shear displacement curves and the axial load N_o vs the shear displacement curve of bolted rock joints with the friction angles of 15˚, 30˚ and 45˚. As can be seen, the increase of the friction angle could increase the global shear loads. The obtained axial load N_o vs shear displacement curves under various friction angles are identical. The friction angle has no impact on the axial force development as smooth joints are

implemented in the analytical model and joint dilation (opening) does not occur during the shearing.

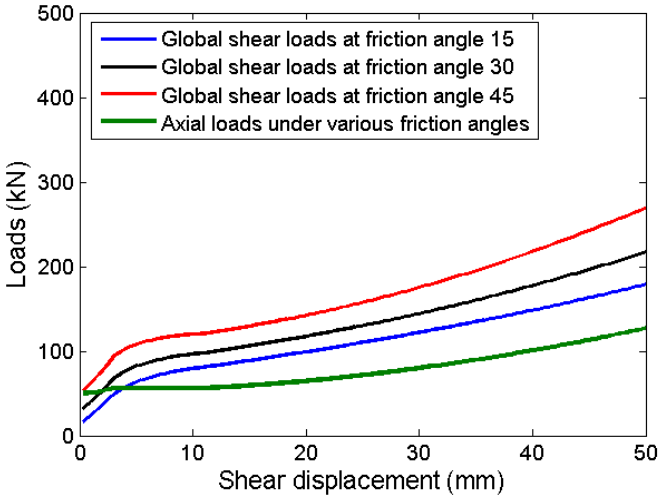

Fig. 27 The global shear load T_b vs shear displacement curves and axial load N_o vs shear displacement curve of bolted rock joints with the friction angles of 15˚, 30˚ and 45˚.

9. Discussions

The bolt axial force evolution, as a function of shear displacement which accounts for pretension forces and the interfacial bond stress, is considered in the proposed analytical model. The axial forces developed in the bolt together with the pretension forces will act as normal forces applying to the joint.

The axial displacements of a bolt installed perpendicularly to the rock joint have not been properly considered in the previous analytical models. For instances, the axial displacement of the bolt is not considered in Ma et al.[21] (2018) and the axial displacement is only considered after the bolt yielding in Pellet and Egger[10] (1996). In the proposed model, the axial displacements of bolts installed perpendicularly to joints are accounted for from the beginning of the loading stage. In addition, the tri-linear tensile stress vs strain curve is used in the model to describe the axial

671 behaviours of the bolt materials. The proposed model is verified by experimental shear tests and
672 the verification shows that the model is able to predict the axial force evolutions of bolts under
673 various pretensions.
674 In the analytical models of Maekawa and Qureshi[18] (1996), Moradi et al.[20] (2012) and Ma et al.[21]
675 (2018), the global shear loads of bolted rock joints are simplified and considered as dowel shear
676 loads of the bolts. In this study, the global shear loads are not equal to the dowel shear loads and
677 are attributed to rock joint roughness, dowel shear loads and axial loads developed in the bolts.
678 The proposed analytical model for predicting the dowel shear load evolution is based on two
679 assumptions:
680 1) The dowel shear load vs the shear displacement curve is assumed to have three stages,
681 which resembles the global shear load-displacement curve obtained from Jalalifar and
682 Aziz[8] (2010b);
683 2) The three stages of the dowel shear load vs the shear displacement curve are associated
684 with the three stages of the tensile stress vs strain curve of the bolt. It is assumed that the
685 dowel shear load and the axial load enter into their respective second stage simultaneously
686 and enter into their respective third stage simultaneously. This assumption saves the trouble
687 of determining the thresholds of the three stages for the dowel shear load vs displacement
688 curve.
689 Comparisons between the experimental results and the analytical model in Figs. 13, 16 and 21
690 show that the predicted global shear loads match well with the experimental results, indicating that
691 the above two assumptions are reasonable and applicable in the analytical modelling.
692 As stated before, the dowel shear load in this study is considered as one of the contributing forces
693 to the global shear load. It can be seen from Figs. 13a, 16a and 21 that the dowel shear loads have

694 the similar values and the increasing trends as the global shear loads, which is due to the fact that
695 the pretension forces are zero in these cases and the developed axial loads are relatively small and
696 have little impacts on the global shear loads. This implies that the dowel shear loads contribute
697 greatly to the global shear loads of the bolted joint, and the dowel shear loads can be used to
698 represent the global shear loads when pretension forces are small. Hence, the shear models of
699 Maekawa and Qureshi[18] (1996), Moradi et al.[20] (2012) and Ma et al.[21] (2018) in which the global
700 shear loads are considered equal to the dowel shear loads remain valid when the pretensions are
701 relatively small.
702
703 **10. Conclusions**
704 An analytical model is proposed in this study for rock joints reinforced by fully grouted rock bolts,
705 with the objective to predict the global shear loads of bolted joints and the axial loads developed
706 in the bolts. The important factors such as the concrete strength, the bolt properties, the bolt profile
707 (the interfacial bond characteristics), the pretensions, bolt inclination angles and joint friction are
708 all taken into account in the model.
709 The proposed analytical model is able to provide complete curves of the dowel shear loads, axial
710 loads, and the global shear loads as function of the joint shear displacement. Available
711 experimental results have been used to verify the proposed analytical model in terms of the global
712 shear load vs the shear displacement curves and the axial load vs the shear displacement curves.
713 Verifications show that the proposed model has the ability to predict the global shear load
714 evolution and the axial load evolution. In addition, the model successfully takes into account the
715 effects of the pretension forces, the concrete strength, the inclination angle and the joint friction.
716

References:

1. Aziz N, Pratt D, Williams R. Double shear testing of bolts. In: Aizz N, ed. *Coal 2003: Coal Operators' Conference.* University of Wollongong & the Australasian Institute of Mining and Metallurgy; 2003:154-161.
2. Bjurstrom S. Shear strength of hard rock joints reinforced by grouted untensioned bolts. *Proceedings of the Congress of the International Society for Rock Mechanics.* 1974:1194-1199.
3. Dight PM. Improvements to the stability of rock walls to open pit mines. Doctor of Philosophy. Melborn: Monash; 1983.
4. Dulacska H. Dowel action of reinforcement crossing cracks in concrete. *Journal of the American Concrete Institute.* 1972;69(12): 754-757.
5. Ferrero AM. The shear strength of reinforced rock joints. *International Journal of Rock Mechanics and Mining Sciences & Geomechanics Abstracts.* 1995;32(6): 595-605.
6. Grasselli G. 3D Behaviour of bolted rock joints: experimental and numerical study. *Int J Rock Mech Min.* 2005;42(1): 13-24.
7. Jalalifar H, Aziz N. Analytical Behaviour of Bolt–Joint Intersection Under Lateral Loading Conditions. *Rock Mech Rock Eng.* 2010a;43(1): 89-94.
8. Jalalifar H, Aziz N. Experimental and 3D Numerical Simulation of Reinforced Shear Joints. *Rock Mech Rock Eng.* 2010b;43(1): 95-103.
9. Jalalifar H, Aziz N, Hadi M. The effect of surface profile, rock strength and pretension load on bending behaviour of fully grouted bolts. *Geotechnical and Geological Engineering.* 2006;24(5): 1203-1227.
10. Pellet F, Egger P. Analytical model for the mechanical behaviour of bolted rock joints subjected to shearing. *Rock mechanic and rock engineering.* 1996;29(2): 73-97.
11. Spang K, Egger P. Action of fully-grouted bolts in jointed rock and factors of influence. *Rock Mech Rock Eng.* 1990;23(3): 201-229.
12. Haas CJ. Analysis of rockbolting to prevent shear movement in fractured ground. *Mining engineering.* 1981;33(6): 698-704.
13. Ludvig B. Shear Tests on Rockbolts. *Proceedings of the International Symposium on Rockbolting.* Abisko, Balkema; 1983:113-123.
14. McHugh E., Signer SD. Roof bolt response to shear stress: laboratory Analysis. *In: Proceedings 18th international conference on ground control in mining, Morgantown, WV.* 1999:232-238.
15. Haile A. A mechanistic evaluation and design of tunnel support systems for deep level South African mines. PhD thesis. University of Natal, Durban, South Africa; 1999.
16. Li L, Hagan PC, Saydam S, Hebblewhite B, Li Y. Parametric Study of Rockbolt Shear Behaviour by Double Shear Test. *Rock Mech Rock Eng.* 2016;49(12): 4787-4797.
17. Bahrani N, Hadjigeorgiou J. Explicit reinforcement models for fully-grouted rebar rock bolts. *Journal of Rock Mechanics and Geotechnical Engineering.* 2017;9(2): 267-280.
18. Maekawa K, Qureshi J. Computational model for reinforcing bar embedded in concrete under combined axial pullout and transverse displacement. *Proceeding of JSCE.* 1996;31(538): 227-239.

19. Soltani M, Maekawa K. Path-dependent mechanical model for deformed reinforcing bars at RC interface under coupled cyclic shear and pullout tension. *Eng Struct.* 2008;30(4): 1079-1091.
20. Moradi AR, Soltani M, Tasnimi AA. A Simplified Constitutive Model for Dowel Action across RC Cracks. *Journal of Advanced Concrete Technology.* 2012;10(8): 264-277.
21. Ma S, Zhao Z, Peng J, Gui Y. Analytical modeling of shear behaviors of rockbolts perpendicular to joints. *Constr Build Mater.* 2018;175: 286-295.
22. Li X, Nemcik J, Mirzaghorbanali A, Aziz N, Rasekh H. Analytical model of shear behaviour of a fully grouted cable bolt subjected to shearing. *Int J Rock Mech Min.* 2015;80: 31-39.
23. Li C, Stillborg B. Analytical models for rock bolts. *Int J Rock Mech Min.* 1999;36(8): 1013-1029.
24. Martin LB, Tijani M, Hadj-Hassen F. A new analytical solution to the mechanical behaviour of fully grouted rockbolts subjected to pull-out tests. *Constr Build Mater.* 2011;25(2): 749-755.
25. Ma S, Nemcik J, Aziz N. An analytical model of fully grouted rock bolts subjected to tensile load. *Constr Build Mater.* 2013;49(0): 519-526.
26. Ma S, Zhao Z, Nie W, Gui Y. A numerical model of fully grouted bolts considering the tri-linear shear bond–slip model. *Tunn Undergr Sp Tech.* 2016;54: 73-80.
27. Jalalifar H. A new approach in determining the load transfer mechanism in fully grouted bolts. PhD thesis. University of Wollongong; 2006.
28. Timoshenko S, Lessels J. *Applied elasticity.* : Pennsylvania:Westinghouse Technical Night School Press; 1925.
29. Dei Poli S, Di Prisco M, Gambarova PG. Shear response, deformation, and subgrade stffness of a dowel bar embedded in concrete. *ACI Journal Structural Journal.* 1992;89(6): 665-675.
30. Marcus H. Load carrying capacity of dowels at transverse pavement joints. *SCI Journal Proceedings.* 1951;48(10): 169-184.
31. Soroushian P, Obaseki K, Rojas MC. Bearing strength and stiffness of concrete under reinforcing bars. *Aci Mater J.* 1987;84(3): 179-184.
32. Neal BG. *The plastic methods of structural analysis. Third Edition.* : Chapmann and Hall, London.; 1977.
33. Aziz NI, Jalalifar H. Experimental and numerical methodology assessment of load transfer capacity of bolts. *Proc. 24th International Conference on Ground Control in Mining.* Morgantown, WV, USA; 2005:285-293.
34. Goris JM, Martin LA, Curtin RP. Shear behavior of cable bolt supports in horizontal, bedded deposits. *In 15th International Conference on Ground Control in Mining.* Colorado School of Mines; 1996:511-521.